Journal of Statistical Physics, Vol. 70, Nos. 5/6, 1993

Kinetic Boundary Layers in Gas Mixtures: Systems Described by Nonlinearly Coupled Kinetic and Hydrodynamic Equations and Applications to Droplet Condensation and Evaporation

M. E. Widder[1] **and U. M. Titulaer**[1]

Received June 10, 1992

We consider a mixture of heavy vapor molecules and a light carrier gas surrounding a liquid droplet. The vapor is described by a variant of the Klein–Kramers equation, a kinetic equation for Brownian particles moving in a spatially inhomogeneous background; the gas is described by the Navier–Stokes equations; the droplet acts as a heat source due to the released heat of condensation. The exchange of momentum and energy between the constituents of the mixture is taken into account by force terms in the kinetic equation and source terms in the Navier–Stokes equations. These are chosen to obtain maximal agreement with the irreversible thermodynamics of a gas mixture. The structure of the kinetic boundary layer around the sphere is then determined from the self-consistent solution of this set of coupled equations with appropriate boundary conditions at the surface of the sphere. For this purpose the kinetic equation is rewritten as a set of coupled moment equations. A complete set of solutions of these moment equations is constructed by numerical integration inward from the region far away from the droplet, where the background inhomogeneities are small. A technique developed in an earlier paper is used to deal with the severe numerical instability of the moment equations. The solutions so obtained for given temperature and pressure profiles in the gas are then combined linearly in such a way that they obey the boundary conditions at the droplet surface; from this solution source terms for the Navier–Stokes equation of the gas are constructed and used to determine improved temperature and pressure profiles for the background gas. For not too large temperature differences between the droplet and the gas at infinity, self-consistency is reached after a few iterations. The method is applied to the condensation of droplets from a supersaturated vapor, where small but significant corrections to an earlier, not fully consistent version of the theory are found, as well as to strong evaporation of droplets

[1] Institut für Theoretische Physik, Johannes-Kepler-Universität Linz, A-4040 Linz, Austria.

0022-4715/93/0300-1255$07.00/0

under the influence of an external heat source, where corrections of up to 40% are obtained.

KEY WORDS: Kinetic boundary layers; droplet condensation; weak and strong evaporation; moment equations; Brownian motion.

1. INTRODUCTION AND SURVEY

Kinetic boundary layers occur in gases or gas mixtures near the surface of a body that can exchange particles, momentum, or energy with the gas.[1] For systems described by linear kinetic equations with space-independent collision operators, accurate analytical and numerical methods have been developed for determining the structure of such layers, especially for essentially one-dimensional geometries (ref. 1–5 and papers quoted therein). The accuracy to which physical quantities of interest can be determined from linear kinetic equations by now far exceeds the accuracy to which these equations themselves apply, even in cases in which nonlinear effects can be expected to be small. In order to make further progress, the incorporation of at least some nonlinear effects is therefore necessary.

In a previous paper,[6] hereafter denoted by I, a first step in this direction was made. The specific problem considered in I was the growth of a small liquid droplet immersed in a mixture of its supersaturated vapor and a light inert carrier gas. The vapor was described by means of the Klein–Kramers equation,[7] the kinetic equation for a collection of Brownian particles, with additional terms[8] to describe the effects of the temperature gradient caused by the release of heat of condensation by the vapor particles absorbed by the droplet. The temperature profile in the background gas was in turn calculated by solving the stationary heat conduction equation for the pure gas with a source term at the droplet surface proportional to the net current of vapor particles. The Klein–Kramers equation with a space-dependent collision operator (and with a force term designed to incorporate thermodiffusion) was transformed into a set of coupled moment equations. These were then integrated numerically, with special procedures developed to overcome the severe numerical instabilities inherent in the system.

In the present paper, a more consistent treatment of the same physical system is developed. In Section 2 we introduce a further generalization of the Klein–Kramers equation that describes a vapor moving in a background with arbitrary temperature and pressure profiles. The force term in this equation is chosen in such a way that the vapor particle current in the Chapman–Enskog solution of this kinetic equation[1,5,9] agrees with the Navier–Stokes expression for a gas mixture.[10] The temperature and

pressure profiles are in turn determined by solving the Navier–Stokes equations for the background gas, with source terms describing the collisional transfer of momentum and energy from the vapor to the background gas, as well as the heat release at the surface. Further details of the iterative procedures used to obtain a consistent solution of the kinetic equation for the vapor and the Navier–Stokes equations for the background gas are given in Section 3; there we also discuss the boundary conditions to be applied at the droplet surface and the approximations used to solve the kinetic equation (which are those used in I with some improvements). In Section 4 we discuss the convergence properties of our scheme with respect to the number of iterations and to the order of the various approximations used in solving the kinetic equations.

In Section 5 we discuss the results obtained by applying our procedure to the droplet condensation problem for which first results, using a preliminary version of the present theory, were already given in I. The parameters of the theory were chosen to correspond to the condensation of mercury vapor in a background of neon. The dependence of the result obtained for the droplet growth rate on the droplet radius and the degree of supersaturation is discussed; the influence of an evaporation coefficient different from unity is also explored. The nonlinear effects for this system turn out to be small, but well in excess of the accuracy obtainable by our method.

In Section 6 we discuss a situation in which larger nonlinear effects occur: the strong evaporation caused by an additional external heat supply to the droplet. We find that reliable results can be obtained by the present version of our method for droplet temperatures up to about 35% above the temperature of the gas mixture at infinity. The final section contains an assessment of the methods developed and the results obtained, as well as an outlook on further possible developments.

2. BASIC EQUATIONS

The Klein–Kramers equation for the distribution function $P(\mathbf{v}, \mathbf{r}, t)$ of the velocities $\mathbf{v}$ and positions $\mathbf{r}$ of an assembly of noninteracting Brownian particles of mass m moving in a background medium with temperature $T = (k\beta)^{-1}$ and undergoing an external force $\mathbf{F}(\mathbf{r})$ reads

$$\left(\frac{\partial}{\partial t} + \mathbf{v} \cdot \frac{\partial}{\partial \mathbf{r}} + \frac{\mathbf{F}(\mathbf{r})}{m} \cdot \frac{\partial}{\partial \mathbf{v}}\right) P = \gamma \frac{\partial}{\partial \mathbf{v}} \cdot \left(\mathbf{v} + \frac{1}{m\beta} \frac{\partial}{\partial \mathbf{v}}\right) P(\mathbf{v}, \mathbf{r}, t) \tag{2.1}$$

where γ denotes the friction coefficient of the particles; β and γ may in general depend on $\mathbf{r}$. By applying the Chapman–Enskog solution

procedure,[5,9] one obtains for the relation between current density $\mathbf{j}_B$ and the density n_B of the Brownian particles in a state near local equilibrium

$$\mathbf{j}_B(\mathbf{r}) = -\frac{1}{m\gamma(\mathbf{r})}\left[\frac{\partial}{\partial \mathbf{r}}\frac{n_B(\mathbf{r})}{\beta(\mathbf{r})} - \mathbf{F}(\mathbf{r})\, n_B(\mathbf{r})\right] \tag{2.2a}$$

In this paper we shall use (2.1) to describe vapor particles with density $n_V(\mathbf{r})$ moving in a background gas of density $n_G(\mathbf{r})$. If we introduce the total density $n = n_V + n_G$ and the associated ideal gas pressure $p = n/\beta$, we can rewrite (2.2a) as

$$\mathbf{j}_V = -\frac{n}{m\beta\gamma}\left(\frac{\partial}{\partial \mathbf{r}}\frac{n_V}{n} + \frac{n_V}{n}\frac{\partial}{\partial \mathbf{r}}\ln p - \mathbf{F}\frac{n_V}{p}\right) \tag{2.2b}$$

The phenomenological quantities γ and $\mathbf{F}$ are now chosen in such a way that the hydrodynamic relation (2.2b) becomes identical to the expression obtained from the hydrodynamics for a gas mixture in which the background component is at rest. In such a mixture the vapor velocity $\mathbf{c}_V \equiv \mathbf{s} + \mathbf{V}_V$, where $\mathbf{s}$ is the hydrodynamic velocity and $\mathbf{V}_V$ is the diffusion velocity, is related to $\mathbf{s}$ by $\mathbf{s} = \mathbf{c}_V \rho_V/\rho$, where ρ_i denotes the mass density of component i. For the vapor current $\mathbf{j}_V$ one then obtains from hydrodynamics[11]

$$\begin{aligned}\mathbf{j}_V &= n_V \mathbf{c}_V \\ &= \frac{n_V \rho}{\rho_G}\mathbf{V}_V \\ &= -n_V \frac{n^2}{\rho_V \rho_G} m_V m_G D_{12}\left[\frac{d}{d\mathbf{r}}\frac{n_V}{n} + \left(\frac{n_V}{n} - \frac{\rho_V}{\rho}\right)\frac{d}{d\mathbf{r}}\ln p + \alpha_T \frac{n_V n_G}{n^2}\frac{d}{d\mathbf{r}}\ln T\right]\end{aligned} \tag{2.3}$$

where D_{12} is the binary diffusion coefficient and α_T the thermal diffusion factor. We can therefore obtain agreement between (2.2b) and (2.3) by choosing

$$\gamma = \frac{n_G}{n}\frac{1}{m_V \beta D_{12}} \tag{2.4}$$

$$\mathbf{F} = -k\alpha_T \frac{n_G}{n}\frac{d}{d\mathbf{r}}T + \frac{m_V}{\rho}\frac{d}{d\mathbf{r}}p \tag{2.5}$$

In the remainder of this paper we shall use (2.1) only for stationary, spherically symmetric problems. In such cases the relevant variables are the magnitudes of $\mathbf{v}$ and $\mathbf{r}$ and the direction cosine $\mu = \hat{\mathbf{v}} \cdot \hat{\mathbf{r}}$.

The background gas is described by the stationary Navier–Stokes equations for a gas at rest, with source terms describing energy and momentum transfer from the vapor atoms. The latter quantities are equal to minus the divergence of the "heat current" and "pressure tensor" of the vapor, evaluated in the rest frame (the actual heat current and pressure tensor should be evaluated in the frame moving with $\mathbf{c}_V$). If we take radial symmetry into account, we obtain from the heat conduction equation, by integrating once with respect to r, an equation for the gas temperature T_G:

$$\lambda_G \frac{dT_G}{dr} = q_r + \frac{c}{r^2} \tag{2.6}$$

where λ_G is the heat conductivity of the gas and c an integration constant. In the pressure equation all convective and viscous terms vanish and the radial variation of the gas pressure equals minus the radial component of the divergence of the "pressure tensor" $\mathbf{\Pi}$. If we evaluate the latter in polar coordinates, use the fact that only Π_{rr} and $\Pi_{\theta\theta} = \Pi_{\phi\phi}$ are nonvanishing, and express the latter in terms of Π_{rr} and $\mathrm{tr}\{\mathbf{\Pi}\} = 3n_V kT_V$, with T_V the vapor "temperature" evaluated in the rest frame, we obtain

$$\frac{dp_G}{dr} = -\frac{d}{dr}\Pi_{rr} + \frac{1}{r}(3n_V kT_V - 3\Pi_{rr})] \tag{2.7}$$

The explicit expressions for q_r, Π_{rr}, and $\frac{3}{2}n_V kT_V$ are

$$q_r(r) = 2\pi \int_0^\infty dv\, v^2 \int_{-1}^{+1} d\mu\, \tfrac{1}{2} m_V v^2 v\mu P(v, r, \mu) \tag{2.8a}$$

$$\Pi_{rr}(r) = 2\pi \int_0^\infty dv\, v^2 \int_{-1}^{+1} d\mu\, m_V v^2 \mu^2 P(v, r, \mu) \tag{2.8b}$$

$$\tfrac{3}{2}n_V kT_V = 2\pi \int_0^\infty dv\, v^2 \int_{-1}^{+1} d\mu\, \tfrac{1}{2} m_V v^2 P(v, r, \mu) \tag{2.8c}$$

As we shall always consider situations in which the gas mixture far away from the droplet is in equilibrium with densities $n_{G\infty}$ and $n_{V\infty}$ and temperature T_∞, it is convenient to choose T_∞ as the unit of temperature and to replace all temperatures T_i by relative temperatures $t_i = T_i/T_\infty$, and to express velocities and lengths in terms of the thermal vapor velocity v_{th} and the velocity persistence length l at infinity; these quantities are

$$v_{\mathrm{th}} = (kT_\infty/m_V)^{1/2}; \qquad l = v_{\mathrm{th}}/\gamma_\infty \tag{2.9}$$

where γ_∞ is the quantity (2.4) evaluated with T_∞, $n_{G\infty}$, and $n_{V\infty}$. The quantities q_r, λ_G, Π_{rr}, p, n, and ρ are henceforth understood to be

expressed in this system of units (e.g., q_r in units of $v_{\text{th}} kT_\infty l^{-3}$) without change of notation. Equations (2.6), (2.7), and (2.1) with (2.5) substituted then read

$$\lambda_G \frac{dt_G}{dr} = q_r + \frac{c}{r^2} \tag{2.10a}$$

$$\frac{dp_G}{dr} = -\frac{d}{dr}\Pi_{rr} + \frac{3}{r}(n_V t_V - \Pi_{rr}) \tag{2.10b}$$

$$v\mu \frac{\partial}{\partial r} P = \left[-v \frac{1-\mu^2}{r} \frac{\partial}{\partial \mu} + \frac{\gamma}{\gamma_\infty} \frac{\partial}{\partial \mathbf{v}} \cdot \left(\mathbf{v} + \frac{\partial}{\partial \mathbf{v}} \right) + (t-1) \frac{\gamma}{\gamma_\infty} \nabla_{\mathbf{v}}^2 \right.$$
$$\left. + \left(\frac{n_G}{n} \alpha_T \frac{dt}{dr} - \frac{1}{\rho} \frac{dp}{dr} \right) \left(\mu \frac{\partial}{\partial v} + \frac{1-\mu^2}{v} \frac{\partial}{\partial \mu} \right) \right] P(v, \mu, r) \tag{2.11}$$

For t and p in (2.11) we substitute the expressions

$$p = p_G + n_V t_V; \qquad t = \frac{n_V t_V + n_G t_G}{n_V + n_G} \tag{2.12}$$

This involves two approximations. First, the expression T_V in (2.8c) is not the vapor temperature, since it is evaluated in the wrong frame, and the simple "mixing laws" (2.12) do not apply for mixtures with components that move relative to one another. However, since we are only considering cases with

$$m_V \gg m_G \qquad \text{and} \qquad \rho_V = m_V n_V \ll m_G n_G = \rho_G \tag{2.13}$$

in which, moreover, the hydrodynamic velocities are much smaller than the thermal ones, such errors are always negligible. Second, the use of the ideal gas equation of state for the vapor used in (2.12) and the interpretation of t_V as a temperature are allowed only near local equilibrium, but not in the kinetic boundary layer. The error thus made is somewhat less easy to estimate, but in view of the small weight with which t_V enters into (2.12), the error is again presumably not significant. Further remarks on these points are made in Section 7.

In the numerical examples we shall use for D_{12} and α_T the expressions derived from first-order kinetic theory for a mixture of Lennard-Jones gases. For the quantity γ/γ_∞ this, e.g., implies[12]

$$\frac{\gamma}{\gamma_\infty} = \frac{n_G}{n_{G\infty}} t^{1/2} \frac{\Omega^{(1,1)*}(tT_\infty^*)}{\Omega^{(1,1)*}(T_\infty^*)} \tag{2.14}$$

with $T^* = kT/\varepsilon_{12}$ and $\varepsilon_{12} = (\varepsilon_1 \varepsilon_2)^{1/2}$, with ε_i the well-depth parameter in the Lennard-Jones potential; $\Omega^{(l,r)*}$ denotes the reduced $\Omega^{(l,r)}$ integral for the Lennard-Jones parameters ε_i and σ_i of the two components. For the example mercury in neon we take the values

$$\begin{aligned} \varepsilon_V/k &= 975 \text{ K}, \qquad \sigma_V = 3.10 \text{ Å} \\ \varepsilon_G/k &= 34.9 \text{ K}, \qquad \sigma_G = 2.78 \text{ Å} \end{aligned} \tag{2.15}$$

The choices made for D_{12} and α_T are the same as in I, to which we refer for further details and discussions.

3. THE BOUNDARY VALUE PROBLEM AND ITS SOLUTION

The central task in developing a theory of droplet condensation and evaporation is the solution of the coupled set of equations (2.10) and (2.11), with the auxiliary definitions (2.8) and (2.12), for given boundary conditions at infinity and at the droplet surface $r = R$. From the half-range completeness property of the fundamental solutions,[1,13] which was proven for the planar case with homogeneous background, and which we assume to hold in the present case as well, we expect that the solution of (2.11) is uniquely determined when $P(v, \mu, R)$ for $\mu > 0$ and the limiting density for $r \to \infty$ are specified. For definiteness we shall assume in this section that the surface $r = R$ behaves as a "black droplet,"[1,4] i.e., that it absorbs all vapor molecules impinging upon it and emits vapor particles with a Maxwellian distribution at the droplet temperature t_D and with the corresponding saturation density $n_S(t_D)$. Hence we impose the boundary conditions

$$P(v, \mu, R) = n_S(t_D)\, \Phi_0(v; t_D) \qquad \text{for} \quad \mu > 0 \tag{3.1a}$$

$$\Phi_0(v; t_D) = (2\pi t_D)^{-3/2} \exp(-v^2/2t_D) \tag{3.1b}$$

and

$$\lim_{r \to \infty} 2\pi \int_0^\infty dv\, v^2 \int_{-1}^{+1} d\mu\, P(v, \mu, r) = n_{V\infty} \tag{3.1c}$$

The solution of (2.10) is determined once we specify $p_{G\infty} = n_{G\infty}$, $t_{G\infty} = 1$, and $t_G(R)$, which can be used to determine the integration constant c in (2.10a). The limiting temperature $t_G(R)$ cannot be put equal to t_D due to the temperature slip phenomenon. For the temperature slip we use the results obtained in an earlier paper[15] for a gas of Maxwell molecules.

The results of ref. 15 for large R can be described for sufficiently small $t_D - 1$ by the asymptotic expression

$$t_G(R) = \tau_1(R) = 1 - \frac{t_D - 1}{1 + 2.7713\tilde{R}^{-1} + 4.97\tilde{R}^{-2} - 2\tilde{R}^{-3}} \tag{3.2a}$$

with $\tilde{R} = R/l_G$ and l_G the mean free path of the gas, evaluated at $t_G = 1$ and $n_G = n_{G\infty}$. For small R, the results of ref. 15 can be fitted by

$$t_G(R) = \tau_2(R) = 1 - (t_D - 1)(-0.205\tilde{R} + 0.019\tilde{R}^2 - 0.0004\tilde{R}^3) \tag{3.2b}$$

In our calculation we used $\tau_1(R)$ for $\tilde{R} > 5.75$ and $\tau_2(R)$ for $\tilde{R} < 1.75$; in the intermediate range, the data of ref. 15 are well reproduced by the interpolating expression

$$t_G(R) = \tfrac{1}{4}[(\tilde{R} - 1.75)\,\tau_1(R) + (5.75 - \tilde{R})\,\tau_2(R)] \tag{3.2c}$$

The expressions (3.2), which are linear in $(t_D - 1)$, are sufficiently accurate for the cases considered in the next two sections; in Section 6, where we shall consider larger values of $t_D - 1$, a more sophisticated way to use the results of ref. 15 will be proposed.

Equations (2.10) and (2.11) will be solved by numerically integrating inward from large r. In practice, one must start at a finite $R_+ \gg R$; to obtaion a definite starting point we shall first solve the modified problem in which $t(r)$ and $p(r)$ assume their limiting values $t(r) = 1$ and $p(r) = n_\infty$ for all $r > R_+$; the limit $R_+ \to \infty$ must afterward be taken, in a way to be discussed in the next section. For $r > R_+$, (2.11) then reduces to

$$v\mu \frac{\partial}{\partial r} P = \left[-v \frac{1 - \mu^2}{r} \frac{\partial}{\partial \mu} + \frac{\partial}{\partial \mathbf{v}} \cdot \left(\mathbf{v} + \frac{\partial}{\partial \mathbf{v}} \right) \right] P \tag{3.3}$$

The solutions of (3.3) have been discussed extensively elsewhere.[5] For large r a solution obeying (3.1c) must have the form

$$P(v, \mu, r) = n_{V\infty} \Phi_0(v; 1) + \alpha_C P^{(C)}(v, \mu, r) + \mathcal{O}[\exp(-R_+/R)] \tag{3.4a}$$

with $P^{(C)}$ the current-carrying Chapman–Enskog solution, which has the moments

$$\begin{gathered} \Pi_{rr}^{(C)} = \frac{2}{r^3} + \frac{1}{r}; \qquad n_V t_V^{(C)} = \frac{1}{r} \\ j_r^{(C)} = 2\pi \int_0^\infty dv\, v^2 \int_{-1}^{+1} d\mu\, v\mu P^{(C)} = \frac{1}{r^2}; \qquad n_V^{(C)} = \frac{1}{r} \end{gathered} \tag{3.4b}$$

If we neglect the exponential terms in (3.4a), then (2.10b) for $r > R_+$ reads

$$\frac{d}{dr}\, p_G = -\frac{d}{dr}\left[n_{V\infty} + \alpha_C \left(\frac{2}{r^3} + \frac{1}{r} \right) \right] - 6\frac{\alpha_C}{r^4} = \frac{\alpha_C}{r^2} \tag{3.5a}$$

with the solution

$$p_G(r) = p_{G\infty} - \frac{\alpha_C}{r} \qquad (r > R_+) \tag{3.5b}$$

For the total pressure we obtain from (2.12)

$$p(r) = p_{G\infty} - \frac{\alpha_C}{r} + p_{V\infty} + \frac{\alpha_C}{r} = p_{G\infty} + p_{V\infty} \qquad (r > R_+) \tag{3.6}$$

whereas for $t(r)$ we find $t(r) = 1$ for all $r > R_+$. Hence the starting assumptions (constant p and t) are satisfied by our solution, and our starting assumptions for $r > R_+$ are consistent.

By further integrating (2.10a, b) inward we obtain

$$t_G(r) = 1 + \int_{R_+}^{r} \frac{1}{\lambda_G} \left(q_r + \frac{c}{r^2} \right) dr \qquad (r < R_+) \tag{3.7a}$$

$$p_G(r) = p_{G\infty} - \frac{\alpha_C}{R_+} - \Pi_{rr}(r) + \Pi_{rr}(R_+) + \int_{R_+}^{r} \frac{3}{r} (n_V t_V - \Pi_{rr})\, dr \tag{3.7b}$$

The constant c can be determined from (3.2) and is given by

$$c = \left[t_G(R) - 1 - \int_{R_+}^{R} \frac{q_r}{\lambda_G}\, dr \right] \Big/ \left(\int_{R_+}^{R} \frac{1}{\lambda_G r^2}\, dr \right) \tag{3.7c}$$

For λ_G we use the first-order kinetic expression for the thermal conductivity of a simple Lennard-Jones gas, (8.2–31) of ref. 12, at a temperature t_G equal to unity in the first iteration and equal to the previous value of $t_G(r)$ in all subsequent ones.

As a first step toward a consistent solution of (2.10) and (2.11) we solve (3.7) with the input functions $n_V(r) = q_r(r) = \Pi_{rr}(r) = \alpha_C = 0$. The resulting expressions for $p(r)$ and $t(r)$ are then substituted into (2.11), which is then solved in a way to be described presently, yielding values for α_C, $n_V(r)$, $q_r(r)$, $\Pi_{rr}(r)$, and $t_V(r)$ that are in turn substituted into (3.7); the procedure is repeated until a sufficient degree of self-consistency is reached.

To solve (2.11) we use a slight modification of the procedure discussed extensively in I. First we expand P in terms of the Burnett functions $\psi_{nk}(v, \mu)$:

$$P(v, \mu, r) = \Phi_0(v; 1) \sum_{n,k=0}^{\infty} b_{nk}(r)\, \psi_{nk}(v, \mu) \tag{3.8}$$

By using the properties of the ψ_{nk}, (2.11) can then be transformed into an infinite set of coupled ordinary differential equations for the $b_{nk}(r)$. For practical calculations this set must be truncated; in contrast to I, we now use the sequence of truncation prescriptions

$$R_N: \quad b_{nk}=0 \qquad \text{for} \quad k \geqslant 2\left[\frac{N-n}{2}\right]+2 \tag{3.9}$$

where $[x]$ denotes the integer part of x. In a notation similar to the one used in I, the truncated set of equations can be written as

$$\mathbb{S}_0 \cdot \frac{d}{dr}\mathbf{b}=\left[-\frac{1}{r}\mathbb{S}_1+\frac{\gamma}{\gamma_\infty}\mathbb{C}_0+(t-1)\frac{\gamma}{\gamma_\infty}\mathbb{C}_1 + \left(\frac{n_G}{n}\alpha_T\frac{dt}{dr}-\frac{1}{\rho}\frac{dp}{dr}\right)\mathbb{T}\right]\cdot\mathbf{b}\equiv\mathbb{V}\cdot\mathbf{b} \tag{3.10}$$

with $\mathbf{b}$ a vector containing the b_{nk} and the space-independent matrices $\mathbb{S}_0$, $\mathbb{S}_1$, $\mathbb{C}_0$, $\mathbb{C}_1$, and $\mathbb{T}$ defined as in I, apart from the different truncation. Due to the new truncation prescription $\mathbb{S}_0$ is regular (the truncated set contains equal numbers of even and odd moments in k), and (3.10) can be recast in the form

$$\frac{d}{dr}\mathbf{b}=\mathbb{S}_0^{-1}\cdot\mathbb{V}\cdot\mathbf{b} \tag{3.11}$$

We now integrate the set of equations (3.11) numerically inward from $r=R_+$, starting with the set of semianalytical Chapman–Enskog and interior boundary layer solutions of the truncated version of (3.3). Using the regularization procedure described and tested in I, we so obtain the Chapman–Enskog and interior boundary layer solutions of (3.10) at $r=R$. Due to the discontinuities in the derivations of p and t at $r=R_+$, a kinetic boundary layer with an admixture of exterior boundary layer solutions occurs near $r=R_+$, but these admixtures have died out as one reaches $r=R$ if R_+ is chosen sufficiently large, and the effects of this spurious boundary layer vanish in any case for $R_+\to\infty$. We then form the unique linear combination of these fundamental solutions, with a coefficient $n_{V\infty}$ multiplying the equilibrium solution, and α_C multiplying the current solution, that satisfies the boundary condition (3.1a) in the Marshak approximation[6,15]

$$\int_{\mu>0} v^2\,dv\,d\mu\,P(v,\mu,R)\,\psi_{n,2k+1}(v,\mu) = \int_{\mu>0} v^2\,dv\,d\mu\,n_S(t_D)\,\Phi_0(v;t_D)\,\psi_{n,2k+1}(v,\mu) \qquad \text{for} \quad n+2k\leqslant N \tag{3.12}$$

In particular, there is just one value of α_C for which such a solution exists. This value of α_C, and the moments $n_V(r)$, $q_r(r)$, $\Pi_{rr}(r)$, and $t_V(r)$, are then used to start the next iteration, starting with (3.7). As we shall show in the next section, the procedure converges rapidly, and sufficiently accurate data for a given N and R_+ are obtained after five iterations.

4. CONVERGENCE PROPERTIES

In the solution scheme for the coupled hydrodynamic and kinetic equations (2.10) and (2.11) with given boundary conditions at the droplet and at infinity, as outlined in the preceding section, we must make three basic approximations: the iterative solution of (2.10) and (2.11) must be broken off after L loops; one must choose a cutoff radius R_+ beyond which the pressure and temperature are assumed to be constant; finally, a cutoff index N must be chosen for the system of coupled moment equations, as specified in (3.9). In principle, the exact solution of our problem should emerge in the limit in which L, R_+, and N all approach infinity. To obtain an estimate for the choices to be made for these cutoff parameters in the calculations to be presented in Section 5 and 6, we present here the result of calculations for a single set of parameters, but with varying choices for L, R_+, and N, in order to check the convergence of our method and to provide extrapolation procedures to estimate the limit L, R_+, $N \to \infty$.

As our parameters we choose $T_\infty = 483.15\,\mathrm{K}$, $t_D = 1.15$, $n_\infty = 100 n_S(T_\infty)$, $n_{V\infty} = 3 n_S(T_\infty)$, and $R = 5l$. For the two gases we choose Lennard-Jones gases with parameters corresponding to mercury and neon, as explained more fully in I and in Section 2. The physical quantity used to measure the convergence properties is the growth rate of the mercury droplet,

$$\dot{R} = -j_r(R)/n_l \tag{4.1}$$

where n_l is the density of liquid mercury at the droplet temperature and pressure, and $j_r(R)$ is the radial vapor current density at the droplet surface, as defined in (3.4).

The dependence on the number of iteration loops L can be seen from the data in Table I. There we list values for $\dot{R}$ obtained for $N = 2$, $R_+ = 10l$ and $N = 4$, $R_+ = 100l$, for values of L from 1 to 6. In both cases the relative difference between $L = 5$ and $L = 6$ is of the order 10^{-8}. Hence we shall use the $L = 5$ approximation in all calculations in the remainder of this section.

In Table II we show the dependence of $\dot{R}$ upon R_+ for $L = 5$ and

Table I. The Dependence of the Growth Rate $\dot{R}(R=5/)$ on the Number of Iteration Loops L, Calculated in R_2 Approximation for $R_+=10$ and in R_4 Approximation for $R_+=100$

	$\dot{R}\times 10^5$	
L	$N=2/R_+=10$	$N=4/R_+=100$
1	−0.8198342498	−0.8248240147
2	−0.7963935609	−0.8063344197
3	−0.7969680885	−0.8065178658
4	−0.7969611727	−0.8065309312
5	−0.7969612464	−0.8065304944
6	−0.7969612472	−0.8065304966

Table II. The Dependence of $\dot{R}(R=5/)$ on R_+, for $L=5$ and $N=2$, 4, 6, 8, and 10, Together with the Four-Parameter Fit (4.2), Using Four Consecutive Values of the Respective Upper Column

	$\dot{R}\times 10^5$				
R_+	$N=2$	$N=4$	$N=6$	$N=8$	$N=10$
10	−0.79696125	−0.79156873	−0.78879824	−0.78724268	−0.78635162
20	−0.80582440	−0.80003111	−0.79717069	−0.79557536	−0.79466156
30	−0.80860353	−0.80270998	−0.79982004	−0.79821073	−0.79728867
40	−0.81000261	−0.80406106	−0.80115614	−0.79953959	−0.79861326
50	−0.81084803	−0.80487816	−0.80196415	−0.80034317	−0.79941422
60	−0.81141466	−0.80542608	−0.80250596		
70	−0.81182104	−0.80581916	−0.80289465		
80	−0.81212676	−0.80611493	−0.80318712		
90	−0.81236513	−0.80634558	−0.80341519		
100	−0.81255620	−0.80653049	−0.80359804		
Four-parameter fit					
	−0.81435091	−0.80826289	−0.80531134	−0.80367176	−0.80273203
	−0.81429889	−0.80821766	−0.80526626	−0.80362687	−0.80268689
	−0.81429352	−0.80821289	−0.80526148		
	−0.81429354	−0.80821236	−0.80526102		
	−0.81429114	−0.80820972	−0.80525898		
	−0.81429333	−0.80821295	−0.80526078		
	−0.81429122	−0.80821119	−0.80526180		

$N = 2, 4, 6, 8$, and 10 for several values of R_+ between $10l$ and $100l$. Also given are estimates for $\dot{R}_\infty$ obtained from four-parameter fits of the type

$$\dot{R}(R_+) = \dot{R}_\infty + c_1 R_+^{-1} + c_2 R_+^{-2} + c_3 R_+^{-3} \tag{4.2}$$

for four successive values of R_+. From the results for lower N we see that the fit from $R_+ = 20, 30, 40, 50l$ has a relative accuracy of 10^{-5}. Since the discrepancy between the first two fits is similar for the higher values of N, this estimate presumably holds for these higher N as well.

In Table III we list the data so obtained for $N = 2, 4, 6, 8$, and 10, and separately those for $N = 3, 5, 7$, and 9. Also given are the estimates $\dot{R}_\infty$ obtained from the three-parameter fit

$$\dot{R}_N(\infty) = \dot{R}_\infty + cN^{-\delta} \tag{4.3}$$

using three successive even or odd N. For even N the values for $\dot{R}_\infty$ are monotonically *increasing*; for odd N they *decrease* monotonically. If we take the last values in each sequence as lower and upper bond, respectively, the final estimate becomes

$$\dot{R}_\infty = -0.79970 \pm 0.00015 \tag{4.4}$$

corresponding to a relative accuracy of 2×10^{-4}. Values for $L = 1$ and $N = 11, 12$ were also obtained; they are consistent with the picture sketched above. Since the errors remaining in the $N \to \infty$ extrapolation are at least an order of magnitude larger than those resulting from the L and R_+ cutoffs, the latter error estimate also holds for the procedure as a whole.

Table III. $\dot{R}_N(R_+ = \infty)$ for $N = 2, 4, 6, 8, 10$ and $N = 3, 5, 7, 9$, and $\dot{R}_\infty$, Obtained from the Three-Parameter Fit (4.3), Using Three Successive Even- or Odd-N Approximations

N	$\dot{R} \times 10^5$	N	$\dot{R} \times 10^5$
2	−0.81429889	3	−0.81381205
4	−0.80821766	5	−0.80691172
6	−0.80526626	7	−0.80441016
8	−0.80362687	9	−0.80313947
10	−0.80268689		
Three-parameter fit:			
	−0.78512130		−0.80018446
	−0.79629497		−0.79985058
	−0.79955337		

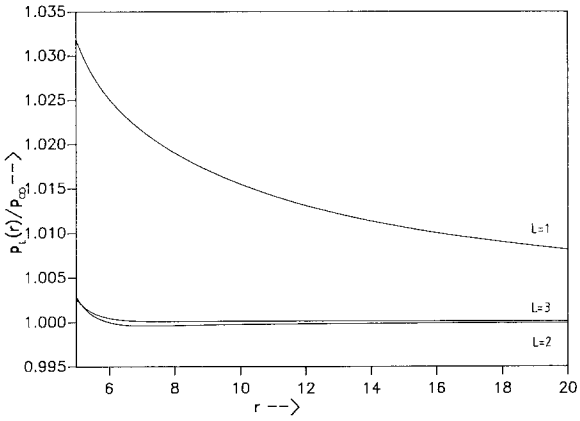

Fig. 1. The total pressure $p_L(r)$ for $L = 1, 2$, and 3 in the vicinity of a droplet with radius $R = 5l$.

In addition to the values for $\dot{R}$, we also considered the convergence with respect to L of the hydrodynamic pressure and temperature profiles $p(r)$ and $t(r)$. Both converge rapidly with L. Due to the large thermal conductivity of Ne, the temperature profile hardly changes as L is increased; the total pressure, shown in Fig. 1, becomes nearly constant for higher L values, as expected from hydrodynamics, with small deviations, of the order of 0.25%, inside the boundary layers. Some further data on the hydrodynamic fields are given in Section 6.

5. THE DROPLET CONDENSATION PROBLEM

In the present section we apply the formalism developed in Sections 2 and 3 and tested in Section 4 to the physical problem of droplet condensation, treated in ref. 14 for a pure vapor in the context of a fully linear theory, and in I using a preliminary version of the present formalism. The main difference with the test problem considered in Section 4 is that the droplet temperature is no longer considered as given, but is in principle also treated as a dynamical variable, which develops in time due to the heat of condensation released as vapor condenses, and the heat transported away by the gas mixture. Since the heat conductivity of the liquid is much larger than that of the gas, we may treat the distribution of heat over the droplet as instantaneous, and describe the droplet by a uniform temperature t_D. Moreover, we saw in ref. 14 that for any given droplet radius, t_D approaches an almost stationary value on a time scale on which the droplet radius hardly changes at all. Hence, we shall here determine t_D

from the problem described in the preceding section by requiring that the heat deposited at the droplet by the vapor particles equals the heat carried away by the gas mixture. This condition reads

$$j_r(R)(q_0 - 2t_D) + q_r(R) = \frac{c}{R^2} + q_r(R) \tag{5.1}$$

where q_0 denotes the equilibrium heat of condensation at t_D and c is defined in (2.6) and (3.7). The right-hand side equals minus the heat carried away by the gas mixture, as is clear from (2.6), and the correction term

$$\delta_q \equiv q_r(R) - 2j_r(R)t_D \tag{5.2}$$

takes account of the fact that the vapor particles arriving at the droplet do not have a Maxwellian distribution at t_D, as is assumed in the definition of the equilibrium heat of condensation q_0. Equation (5.1) is an implicit equation for t_D, since c, q_0, q_r, and j_r all depend on the droplet temperature t_D. In Table IV we present the data obtained for t_D and the droplet growth rate $\dot{R}$, defined in (4.1), for $R = 5l$, $T_\infty = 483.15$ K, $n_\infty = 100 n_S(T_\infty)$, and $n_{V\infty} = 3n_S(T_\infty)$. The extrapolations to $N = \infty$ and $R_+ = \infty$ were carried out as described in the preceding section. The first line gives the result obtained in lowest order using the description used in I,[2] i.e., in

[2] The result in the first line differs from the one given in Table IV of I, since in the earlier paper we evaluated the gas mean free path l_G in (3.2a) at the total density of the mixture; in the present paper we used the partial gas density, since the momentum transfer to the vapor is taken into account explicitly in (2.11). Using the procedure in I, we would have obtained $\dot{R} = (0.261883 \pm 0.000002) \times 10^{-5}$; the difference from the value $\dot{R} = (0.2619 \pm 0.0006) \times 10^{-5}$ quoted in I is due to the better convergence of the truncation prescription (3.9) compared to D_N used in I.

Table IV. The Growth Rate $\dot{R}$ and the Droplet Temperature t_D, for $R = 5l$ and $T_\infty = 483.15$ K[a]

$\dot{R} \times 10^5$	t_D	Δ
0.261165 ± 0.000002	1.03492	—
0.257147 ± 0.000005	1.03439	−1.5%
0.256311 ± 0.000002	1.03461	−1.8%
0.253230 ± 0.000070	1.03443	−3.0%

[a] The first line contains the result in lowest order. In the second line all terms in (2.11) are taken into account in the $L = 1$ approximation, without the correction of δ_q. In the third line the additional correction δ_q is taken into account; the last line contains the full $L = 5$ result. The quantity Δ is the percentile change in $\dot{R}$ relative to the number given in the first line.

$L=1$, neglecting the space-dependent terms in (2.11) arising from the inhomogeneity of the background gas, as well as the correction δ_q. In the second line all terms in (2.11) have been taken into account in the $L=1$ approximation, but δ_q is still neglected. In the third line δ_q has been taken into account; the last line contains the full $L=5$ result. The quantity Δ is the respective percentile change in $\dot{R}$ compared to the first line.

In the remainder of this section we study the dependence of the solution on the radius R and the degree of supersaturation as well as the influence of an absorption coefficient different from unity. We shall always first give the results obtained by the crudest approximation (neglecting space dependences in the background and the correction δ_q) and subsequently the corrections following from the more complete and consistent treatment.

In Fig. 2 we show the growth rate $\dot{R}_N^{(0)}$ as a function of R for $N=2$, 4, 6, and 8 in the crude approximation used in the first line of Table IV, with the temperature jump at the surface determined by (3.2). For $R\to 0$ the droplet is no longer able to disturb the equilibrium distribution of the vapor, and the droplet temperature can be determined from

$$q_0[n_S(t_D)\sqrt{t_D}-n_\infty]/(2\pi)^{1/2}=-\lambda_G\alpha_1\frac{l}{l_G}(t_D-1) \tag{5.3}$$

with $\alpha_1=-0.205$ the constant appearing in (3.2b). The value $\dot{R}(0)$ calculated from this t_D is indicated by the arrow in Fig. 2[3]; we see from

[3] The slight discrepancy between Fig. 2 and Table IV is due to the fact that the results in Table IV were obtained using a somewhat too rough numerical interpolation for $n_S(t)$; all further results use the more accurate interpolation used in Fig. 2.

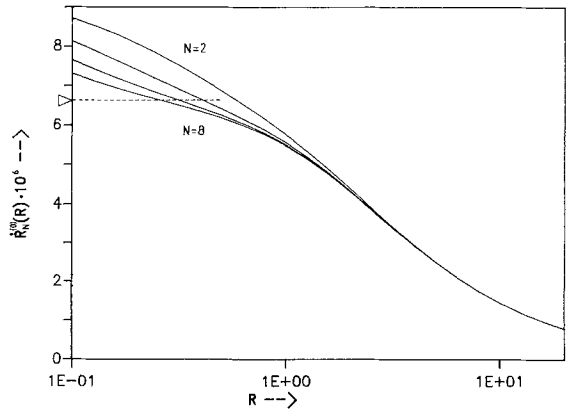

Fig. 2. The growth rate $\dot{R}_N^{(0)}$ in units of v_{th} as function of R, for $N=2$, 4, 6, and 8. The arrow indicates the value for $R\downarrow 0$, calculated via (5.3).

Fig. 2 that the convergence with N is satisfactory, at least for $R \gtrsim 1$. In Fig. 3 we show the relative corrections to this crude approximation due to δ_q and the background inhomogeneities. The dotted upper and lower curves show $\dot{R}_2/\dot{R}_2^{(0)}$ in the $L=1$ and $L=3$ approximations, respectively. The dashed and solid curves correspond to $N=4$ and $N=6$; the long-dashed curve shows the $N \to \infty$ extrapolation $\dot{R}_\infty^{(0)}$, as determined from (4.3), divided by $\dot{R}_6^{(0)}$. Our best estimate for $\dot{R}$ would be obtained by adding this correction to the $L=3$, $N=6$ curve.

The dependence of $\dot{R}^{(0)}$ on the supersaturation $s \equiv [v_{V\infty} - n_S(T_\infty)]/n_S(T_\infty)$ at constant $n_\infty = 100 n_S(T_\infty)$ is approximately linear between $\dot{R}^{(0)}(s=-0.4) = -0.545 \times 10^{-6} v_{\text{th}}$ and $\dot{R}^{(0)}(s=4) = 0.461 \times 10^{-5} v_{\text{th}}$ (for $R = 5l$), with deviations of at most 9%. In Fig. 4 we give the relative deviation $\dot{R}_N/\dot{R}_N^{(0)}$ as a function of the supersaturation for $N=2$ and $L=1$ and $L=3$, as well as the corresponding results for $N=4$ and $N=6$.

To demonstrate the applicability of our formalism to more complicated boundary conditions, we also treated the case of an absorption (and evaporation) coefficient $(1-r)$ different from unity, with specular reflection of the vapor particles that are not absorbed. As in ref. 14, we thus replace (3.1a) by

$$P(v, \mu, R) = (1-r)\, n_S(t_D)\, \Phi_0(v; t_D) + rP(v, -\mu, R) \qquad \text{for} \quad \mu > 0 \qquad (5.4)$$

We refer to ref. 14 for further discussion of this assumption. The growth rate reduction in the crude approximation $\dot{R}_N^{(0)}(r)/\dot{R}_N^{(0)}(r=0)$ for $N=2$ and $N=6$ and $R=0.1$, 1, 5, 20, and 100 and supersaturation $s=2$ is shown in

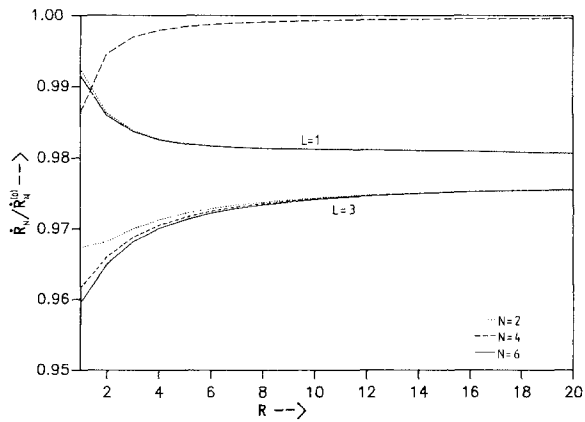

Fig. 3. The growth rate $\dot{R}_N(R)$, including all terms in (2.11) and the correction δ_q, divided by $\dot{R}_N^{(0)}(R)$, in the $L=1$ and $L=3$ approximations. The dotted, dashed, and solid curves correspond to $N=2$, 4, and 6, respectively. The long-dashed curve shows $\dot{R}_\infty^{(0)}/\dot{R}_6^{(0)}$.

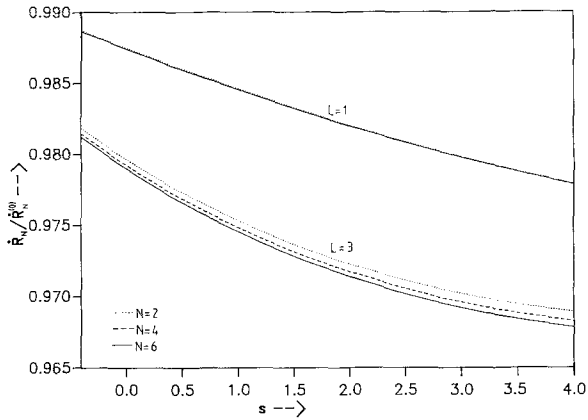

Fig. 4. The relative growth rate $\dot{R}_N/\dot{R}_N^{(0)}$, defined in the caption of Fig. 3, as a function of the supersaturation s, in the $L=1$ and $L=3$ approximations.

Fig. 5. The dashed line is the limiting value for $R\downarrow 0$, obtained from (5.3) with an extra factor of $(1-r)$ multiplying the left-hand side. As in ref. 14, we see a transition from an almost linear dependence on r for small[4] R to a result that is almost independent of r (for r not too close to unity) in the heat-diffusion-controlled regime at $R \gg l$. The "overshoot" of the $R=0.1$

[4] In contrast to ref. 14, the dependence of r for $R\downarrow 0$ is not exactly linear, since the dependence of t_D on r, which was not included in the calculations in ref. 14, is taken into account in the present calculations.

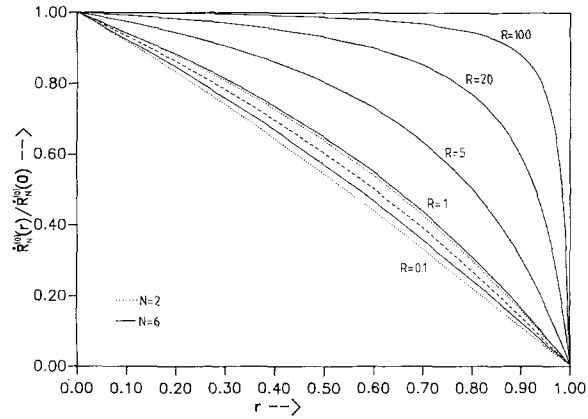

Fig. 5. The lowest order growth rate $\dot{R}_N^{(0)}$ as a function of the reflection coefficient r, divided by the value for $r=0$, for $R=0.1$, 1, 5, 20, and 100, in the $N=2$ (dotted) and $N=6$ (solid) approximations. The dashed line represents the limiting curve for $R\downarrow 0$.

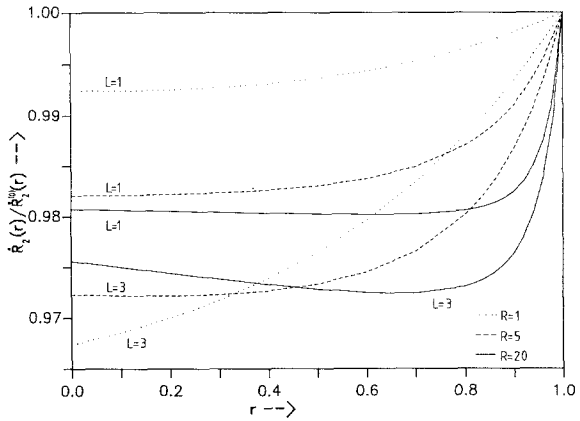

Fig. 6. The relative growth rate $\dot{R}_2(r)/\dot{R}_2^{(0)}(r)$, defined in the caption of Fig. 3, for $R=1$ (dotted), 5 (dashed), and 20 (solid). The upper curves correspond to $L=1$, the lower ones to $L=3$, respectively.

results relative to the $R \downarrow 0$ limit is not numerically significant; the poorer convergence with respect to N as R decreases was already found and analyzed in ref. 5. In Fig. 6 we show the corrections due to δ_q and the inhomogeneities of the background gas in the $L=1$ and $L=3$ approximations for $R=1$, 5, and 20.

6. STRONG EVAPORATION

In the problem considered in the preceding section (sometimes called the weak condensation or evaporation problem), the temperature of the droplet was determined by the balance between the heat of condensation released by the condensing gas and the heat conducted away by the surrounding gas mixture. Due to the steep increase of the saturation density with temperature and to the good heat conductivity of the gas, the droplet temperature never exceeded the temperature at infinity by more than 5%, even at high supersaturation, and the nonlinear effects, though significant, were only moderate in size. This situation may change when additional heat is supplied to or withdrawn from the droplet; this is called the strong evaporation or condensation problem. It is the aim of the present section to explore the extent to which the formalism developed can be used in such a context as well, and to see how large the nonlinear effects may become in such a situation. Rather than attempting an inclusion of external heat sources or sinks into our problem, we return to the case considered in Section 4 and solve the boundary layer problem for a range of relative

droplet temperatures; the determination of the actual temperature can in principle be carried out as in Section 5, or with the techniques of ref. 14 when temperature transients are of interest.

Before describing the results of this program, we introduce a modification of the temperature boundary condition (3.2) that becomes necessary for relative droplet temperatures t_D that differ markedly from unity. The boundary condition (3.2), which can be written in the form

$$T_G(R) = T_\infty + f(R/l_G)(T_D - T_\infty) \tag{6.1}$$

with the mean free path $l_G = l_G(T_\infty, p_{G\infty})$ evaluated for the gas at infinity, was developed in the context of a fully linear treatment, in which the temperature profile $T_G(r)$ takes the form

$$\begin{aligned} T_G(r) - T_\infty + f\left(\frac{R}{l_G}\right)(T_D - T_\infty)\frac{R}{r} \\ \frac{d}{dr}T_G(r) = -f\left(\frac{R}{l_G}\right)(T_D - T_\infty)\frac{R}{r^2} \end{aligned} \tag{6.2}$$

The function f was calculated in ref. 15 from an analysis of the kinetic boundary layer in the gas at low values $t_D - 1 = (T_D - T_\infty)/T_\infty$. For larger $t_D - 1$ it is preferable to consider (6.1) as a relation between the temperature jump $T_D - T_G(R)$ and the hydrodynamic temperature gradient near the droplet surface, and to employ a *local* mean free path as the relevant unit of length. For this purpose we write

$$\begin{aligned} T_G(R; \tilde{T}_\infty) = \tilde{T}_\infty + f\left(\frac{R}{\tilde{l}_G}\right)(T_D - \tilde{T}_\infty) \\ \left.\frac{dT_G(r; \tilde{T}_\infty)}{dr}\right|_{r=R} = -f\left(\frac{R}{\tilde{l}_G}\right)(T_D - \tilde{T}_\infty)R^{-1} \end{aligned} \tag{6.3}$$

with

$$\tilde{l}_G = l_G(\tilde{T}_\infty, p_G(R)) \tag{6.4}$$

with $p_G(R)$ evaluated using (3.7b) and $\tilde{T}_\infty$ a parameter to be determined presently. This expression is compared with the expressions obtained by solving (3.7a):

$$\begin{aligned} T_G^*(R; c) = T_\infty + \int_\infty^R \frac{1}{\lambda_G}\left[q_r(r) + \frac{c}{r^2}\right]dr \\ \left.\frac{d}{dr}T_G^*(r; c)\right|_{r=R} = \frac{1}{\lambda_G}\left[q_r(R) + \frac{c}{R^2}\right] \end{aligned} \tag{6.5}$$

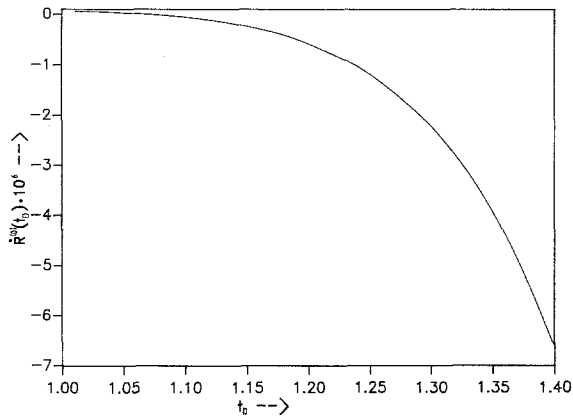

Fig. 7. The lowest order droplet growth rate $\dot{R}^{(0)}$ as a function of the droplet temperature t_D, calculated without the influence of space dependences in the background gas. Negative values of $\dot{R}$ correspond to evaporation.

Note that these expressions contain the free parameter c, which can only be determined when the boundary condition for T_G at $r = R$ is known. The two unknown parameters $\tilde{T}_\infty$ and c are now determined by requiring

$$T_G(R; \tilde{T}_\infty) = T_G^*(R; c); \qquad \frac{d}{dr} T_G(r; \tilde{T}_\infty)\bigg|_{r=R} = \frac{d}{dr} T_G^*(r; c)\bigg|_{r=R} \tag{6.6}$$

where we did not write the indirect dependences on $\tilde{T}_\infty$ and c via the moments of the vapor distribution appearing in (3.7) explicitly; in solving

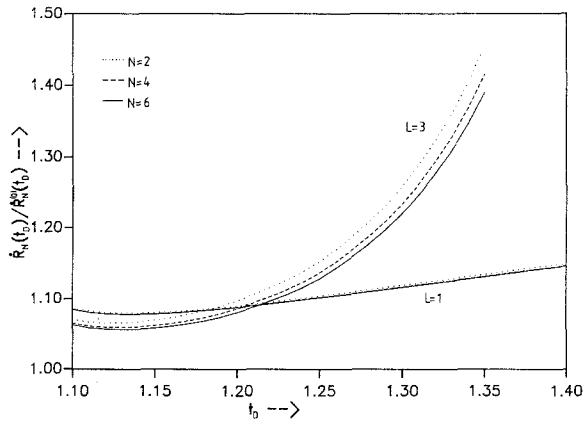

Fig. 8. The relative growth rate $\dot{R}_N(t_D)/\dot{R}_N^{(0)}(t_D)$, as defined in the caption of Fig. 3, in the $L = 1$ and $L = 3$ approximations, for $N = 2$ (dotted), 4 (dashed), and 6 (solid).

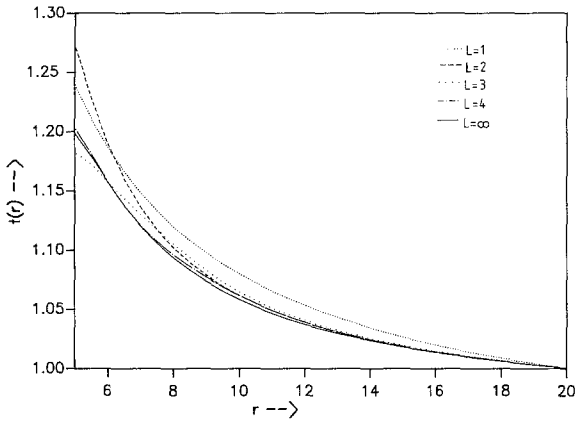

Fig. 9. The temperature profile $t(r)$ in the vicinity of a droplet with radius $R = 5l$, for $t_D = 1.35$ and $L = 1, 2, 3, 4$, and 5. The $L = 5$ and $L = \infty$ profiles do not differ noticeably.

(6.6), which must be done anew in each L iteration, the expressions from the previous iteration loop are used for these moments.

With these modified boundary conditions for $t_G(R)$ we solved the problem of Section 4 for $R = 5l$, $T_\infty = 373$ K, $n_{V\infty} = 3n_S(T_\infty)$, and $n_\infty = 100n_S(T_\infty)$ for $1 < t_D < 1.4$. As expected, the convergence with L becomes slower as t_D increases, and the method as described in Sections 2 and 3 breaks down for droplet temperatures $t_D \gtrsim 1.37$. In Fig. 7 we show the lowest order droplet growth rate $\dot{R}^{(0)}$ as a function of t_D, calculated without the influence of space dependences in the background gas. For high t_D this growth rate becomes negative, i.e., the droplet evaporates under the influence of the externally supplied heat, in spite of the supersaturation. In Fig. 8 we provide data for the correction factor $\dot{R}_N(t_D)/\dot{R}_N^{(0)}(t_D)$ both in the $L = 1$ approximation and in the limit $L \to \infty$ for several N. From the $L = 1$ curves we see that thermal diffusion hinders the emitted particles in returning to the droplet and hence increases the evaporation rate $|\dot{R}|$. The effects due to energy and momentum exchange amount to about 40% at $t_D = 1.35$; they are thus about an order of magnitude larger than in the problem discussed in Section 5. To provide an impression of the convergence with L for high t_D, we show in Fig. 9 the temperature profiles $t(r)$ in the $N = 2$, $R_+ = 20$ approximation for $t_D = 1.35$ and several values of L; the $L \to \infty$ limit is also shown. We see that even for this high value of t_D, the temperature profile has essentially reached its limit for $L = 4$.

7. DISCUSSION AND CONCLUDING REMARKS

The main result of this paper is the development of a formalism that allows one to incorporate a number of the effects of the energy and momentum exchange between the vapor and the background gas into the Klein–Kramers equation and to solve this equation and the Navier–Stokes equations for the background gas in a self-consistent manner. The methods developed in I turned out to be completely sufficient to solve these modified equations as well for the weak condensation and evaporation problem. For the strong evaporation problem, the method designed in I breaks down for temperature differences between droplet and gas in excess of about 37%. One of the reasons for the slow convergence might be the use of Burnett functions adapted to T_∞ in the expansion (3.8). The use of a basis adapted to a spatially varying temperature is possible in principle; it might lead to some extension of the range of applicability of the formalism, but the tests needed to verify this conjecture have not yet been carried out.

In the remainder of this section we discuss the various simplifications made in the course of the development of our method and the extent to which they can be justified or relaxed.

The least problematic assumption involves our use of a *stationary* kinetic equation. The growth rates found for the droplets were always of the order of $(10^{-5}$–$10^{-6})v_{\text{th}}$. The velocity so transferred to the background gas can safely be neglected in the Navier–Stokes equations for the gas. The related assumption in Section 5 of a stationary droplet temperature is less universally valid. However, the case of an initial temperature different from the quasistationary value can be treated[16] using the method described in ref. 14 and applied there to a droplet condensing from a pure vapor.

A number of other physical effects can likewise be incorporated without much difficulty, since they involve merely the boundary conditions imposed at the droplet surface. As examples we mention the dependence of the saturation pressure on the droplet radius due to the surface tension effects[17] or the heat loss due to radiation. Also, the effect of incomplete thermal accommodation of the gas molecules reflected from the surface[14] or of partial energy accommodation of those vapor molecules not absorbed by the droplet can be analyzed in a straightforward manner.

The most serious approximation involves the replacement of the Boltzmann equation for the gas mixture by the modified Klein–Kramers equation for the vapor and the Navier–Stokes equations for the gas. Some of its shortcomings that were still present in I are alleviated in the present paper. Most importantly, the transfer of momentum and energy from the vapor to the gas is now taken into account, at least to within the

approximation that the gas can still be considered in local equilibrium. Moreover, since the force terms in (2.11) involve the pressure and temperature *of the mixture*, the collisions between the vapor molecules are taken into consideration at least to some extent, albeit not in a very realistic way (the Brownian approximation certainly does not apply to collisions between vapor molecules). However, the inequalities that must be satisfied for the Klein–Kramers equation to be valid (high mass ratio between vapor and gas molecules, but a low ratio of the mass densities of vapor and background gas) are never satisfied very well in practical applications, except for very low relative vapor densities; in the latter case, however, the droplet temperature for stationary condensation is even lower than in the cases considered in Section 5, and the nonlinear effects become accordingly less important. Similarly, the condition $l \gg l_G$, which was used to justify neglecting boundary layer effects in the background gas (other than the temperature jump), is fulfilled only moderately well. In order to estimate the errors made by these approximations, the comparisons, should be made either with numerical solutions of the Boltzmann equation[18] for the mixture of Lennard-Jones gases mimicked by our Eq. (2.11) or by similar calculations using different collision operators. Since in earlier calculations[1,5,14] many effects of kinetic boundary layers were found to be surprisingly independent of the collision operator chosen, there is a possibility that the inadequacy of the collision operator might not have too serious consequences in the present case either.

In principle, the method developed in this paper might be used for an arbitrary Boltzmann equation; the general expression

$$\mathscr{S}P + \mathscr{C}(P, P) = 0 \tag{7.1}$$

with $\mathscr{S}$ the streaming operator and $\mathscr{C}$ a bilinear collision operator, may be replaced by the sequence of linear Boltzmann equations

$$\mathscr{S}P_k + \mathscr{C}(P_k, P_{k-1}) = 0 \tag{7.2}$$

with P_0 the local equilibrium distribution. Each of Eqs. (7.2) could be solved using the techniques of I and the present paper, with general boundary conditions at the droplet surface. However, the convergence properties of the sequence (7.2) with increasing k would have to be studied separately for each case. A suitable first example would be a collision operator of BGK type,[1] where $\mathscr{C}$ depends on just a few moments of P_{k-1}.

We applied our method to the spherically symmetric case because for that case accurate results from more elementary theories[2,6,14] are available and because of the practical importance of the droplet condensation

problem. However, the method should be even easier to apply to planar kinetic boundary layers, where the choice of the truncation for the system of moment equations is likely to be less critical. Applications to the cylindrical case, for which the linear theory corresponding to refs. 2, 14, and 15 was recently worked out,[19] should also be feasible, at least for the Boltzmann collision operator. For the Klein–Kramers case, a semianalytic treatment for the case of a linear or logarithmic temperature gradient in the background would have to be developed first, to provide a start for the numerical integrations from $r > R_+$.

ACKNOWLEDGMENT

The work reported in this paper was supported by the Austrian Fonds zur Förderung der wissenschaftlichen Forschung.

REFERENCES

1. C. Cercignani, *Theory and Application of the Boltzmann Equation* (Scottish Academic Press, Edinburgh, 1975); *The Boltzmann Equation and Its Applications* (Springer, New York, 1988).
2. M. E. Widder and U. M. Titulaer, *J. Stat. Phys.* **55**:1109 (1989); **56**:471 (1989).
3. T. W. Marshall and E. J. Watson, *J. Phys. A* **18**:3531 (1985); P. W. Duck, T. W. Marshall, and E. J. Watson, *J. Phys. A* **19**:3545 (1986); T. W. Marshall and E. J. Watson, *J. Phys. A* **20**:1345 (1987).
4. A. J. Kainz and U. M. Titulaer, *J. Phys. A* **24**:4677 (1991); **25**:1855 (1992); to be published (1992).
5. M. E. Widder and U. M. Titulaer, *Physica A* **167**:663 (1990); **173**:125 (1991).
6. M. E. Widder and U. M. Titulaer, *J. Stat. Phys.* **67**:347 (1992).
7. O. Klein, *Ark. Mat. Astron. Fys.* **16**(5):1 (1922); H. A. Kramers, *Physica* **7**:284 (1940).
8. M. E. Widder and U. M. Titulaer, *Physica A* **154**:452 (1989).
9. U. M. Titulaer, *Physica A* **91**:321 (1978); **100**:234 (1980).
10. L. D. Landau and E. M. Lifshitz, *Fluid Mechanics* (Pergamon, Oxford, 1987).
11. J. H. Ferziger and H. G. Kaper, *Mathematical Theory of Transport Processes in Gases* (North-Holland, Amsterdam, 1972).
12. J. O. Hirschfelder, C. F. Curtiss, and R. B. Bird, *Molecular Theory of Gases and Liquids* (Wiley, New York, 1954).
13. R. Beals and V. Protopopescu, *J. Stat. Phys.* **32**:565 (1983).
14. G. F. Hubmer and U. M. Titulaer, *J. Stat. Phys.* **63**:203 (1991).
15. G. F. Hubmer and U. M. Titulaer, *Physica A* **171**:337 (1991).
16. M. E. Widder and U. M. Titulaer, in *Rarefied Gas Dynamics* **19**, to be published.
17. R. Becker, *Theorie der Wärme* (Springer, Berlin, 1985).
18. F. Gropengiesser, H. Neunzert, and J. Struckmeier, Computational methods for the Boltzmann equation in *Applied and Industrial Mathematics Venice-1 1989*, R. Spigler ed. (Kluwer, Dordrecht, 1991).
19. C. Kloimböck and U. M. Titulaer, to be published.